Novel chromosome organization pattern in actinomycetales–overlapping replication cycles combined with diploidy

Kati Böhm[1], Fabian Meyer[1], Agata Rhomberg[1], Jörn Kalinowski[2], Catriona Donovan[1], and Marc Bramkamp[1]*

[1]Ludwig-Maximilians-Universität München, Fakultät Biologie, Großhaderner Straße 2-4, 82152 Planegg-Martinsried, Germany

[2]Universität Bielefeld, Center for Biotechnology (CeBiTec), 33594 Bielefeld, Germany

Keywords: *Corynebacterium*, cell cylce, origin, ParB, ParA, replication, diploidy

*Corresponding author: Marc Bramkamp

Email: marc.bramkamp@lmu.de; Phone: +49-(0)89-218074611; Fax: +49-(0)89-218074621

Abstract

Bacteria regulate chromosome replication and segregation tightly with cell division to ensure faithful segregation of DNA to daughter generations. The underlying mechanisms have been addressed in several model species. It became apparent that bacteria have evolved quite different strategies to regulate DNA segregation and chromosomal organization. We have investigated here how the actinobacterium *Corynebacterium glutamicum* organizes chromosome segregation and DNA replication. Unexpectedly, we find that *C. glutamicum* cells are at least diploid under all conditions tested and that these organisms have overlapping C-periods during replication with both origins initiating replication simultaneously. Based on experimentally obtained data we propose growth rate dependent cell cycle models for *C. glutamicum*.

Introduction

Bacterial chromosome organization is highly regulated, where replication coincides with segregation of sister nucleoids and is tightly coordinated with cell division (1). Cell cycle control mechanisms exist, which ensure constant DNA content throughout cell generations. In particular, the action of the key replication initiator protein DnaA is timed by various regulatory systems, for instance via the CtrA protein cascade in *Caulobacter crescentus* or SeqA in *Escherichia coli* (2-6). Upon replication initiation DnaA binds to the origin of replication (*oriC*) and mediates duplex unwinding prior to loading of the replication machinery (7,8). The two evolving replication forks migrate along the left and right arm of the circular chromosome towards the terminus of

44 replication (*terC*), where FtsK-dependent XerCD recombinases resolve decatenated
45 chromosomes as a final step (9,10). Replication usually takes place within defined
46 cellular regions via stably assembled protein complexes, namely replisomes, of
47 rather static or dynamic nature (11,12).

48 The bacterial cell cycle can be divided in different stages illustrated in Figure 1. The
49 time of DNA-replication is termed C-period, which is followed by a time interval
50 necessary for cell division executed by the divisiome (D-period). Several bacteria like
51 *Mycobacterium smegmatis* and *C. crescentus* replicate their genome once within a
52 generation, where C-periods are temporally separated from each other (13,14). At
53 slow growing conditions a non-replicative state termed B-period precedes the C-
54 period (not shown), thus the bacterial cell cycle resembles in some aspects the
55 eukaryotic cell cycle (G1, S, G2 phases). Contrary to this, fast growing organisms
56 such as *Bacillus subtilis*, *E. coli* and *Vibrio cholerae* can overlap C-periods during fast
57 growth, a phenomenon termed multifork replication (15-17). Under these conditions a
58 new round of replication is reinitiated before termination of the previous one.
59 Therefore, generation times are considerably shorter than the duration of the C-
60 period. However, only one round of replication is initiated per cell cycle and usually
61 one C-period is completed at the time point of cell division (18). Many bacteria
62 contain only one copy of the chromosome. However, several bacteria and archaea
63 can have increased DNA contents due to oligo- or polyploidy (19). Polyploid cells
64 harbor multiple, fully replicated chromosome copies throughout their life cycle, which
65 has been frequently found in prokaryotes including certain gram-positive bacteria,
66 proteobacteria, Deinococcales, cyanobacteria and also archaea (20-27).

67 Besides the distinct cell cycle modes chromosome localization patterns differ
68 between model organisms. In a non-replicating, slow-growing *E. coli* cell the single

chromosome is placed symmetrically with *oriC* and *terC* regions located at midcell and the replichores spatially separated to the two cell halves (28). Upon replication initiation the two sister chromosomes segregate bidirectionally to opposite cell halves with replisomes positioned at midcell (29,30). Finally, *oriC* and *terC* are confined to cell quarter regions. Contrary to this, the model organisms *C. crescentus*, *Vibrio cholerae* and *Pseudomonas aeruginosa* localize their nucleoids about the longitudinal axis with chromosome arms adjacent to each other (31-34). Sister replichores move to the opposite cell half with the segregated *oriC* facing towards the pole, mirroring the second chromosome at the transverse axis. The *oriC* region of *C. crescentus* and *V. cholera* is positioned by polar landmark proteins (35,36), where replisomes assemble and simultaneously move towards midcell in the course of replication (12,17). For the most part, *P. aeruginosa* places its replication machinery centrally (34). Finally, *B. subtilis* switches from the longitudinal chromosome organization to the *E. coli* "left-*oriC*-right" configuration during replication initiation (37).

The mitotic-like ParABS system has been identified as a driving force behind coordinated nucleoid partitioning for more than two third of bacterial species analyzed, with exceptions specifically within the phylum of γ-proteobacteria such as *E. coli* (38). This segregation mechanism involves components similar to the plasmid encoded *par* genes responsible for active segregation of low-copy-number plasmids (39). Thereby, the ParB protein binds a variable number of centromere-like DNA sequences called *parS* sites in *oriC*-proximity (40) and spreads along the DNA forming large protein-DNA complexes (41-43). Interaction of ParB with the Walker-type ATPase ParA mediates ATP-hydrolysis and thereby ParA detachment from DNA (44), driving apart the sister chromosomes as the protein interaction translocates the

oriC towards the opposite cell half (33,45,46). The precise mechanism of the ParABS-mediated DNA segregation has been under debate, however, to date dynamic diffusion-ratchet and DNA-relay models are favored, where nucleoid and plasmid movement is mediated along a ParA gradient caused by local ParB-stimulated depletion of DNA-bound ParA (47-49). Deletion of this partitioning system has mild effects in *B. subtilis* and *V. cholera*e cells, but causes severe chromosome segregation defects in other organisms and is essential for viability in *C. crescentus* and *Myxococcus xanthus* (46,50-56).

Here we present the cell cycle and spatiotemporal organization of *oriCs* and replisomes in *C. glutamicum*, a rod-shaped polar growing actinobacterium. It is closely related to pathogens like *C. diphteriae* and *M. tuberculosis*, the latter being amongst the top ten causes of fatal infections worldwide (57). Besides this, *C. glutamicum* is of great economic importance as an amino acid and vitamin producer and extensive efforts in metabolic engineering are being carried out concerning metabolite production and yield increase (58). Although, its metabolism is one of the best studied amongst model organisms the underlying cell cycle parameters and chromosome organization patterns had so far not been analyzed in detail. *C. glutamicum* relies on a ParABS system to segregate their nucleoids prior to cell division (51,59,60). Chromosome segregation influences division site selection and, hence, growth and chromosome organization are tightly coupled in *C. glutamicum* (59). This may in part explain why protein machineries that have been described in various bacterial species like the Min system or a nucleoid occlusion system, both being involved in division septum placement are absent in *C. glutamicum* (61).

In this study, we tracked *in vivo* fluorescently labeled centromer-binding protein ParB and replisome sliding clamp DnaN to investigate spatiotemporal *oriC* and replisome

119 localization throughout the cell cycle. Fluorescence microscopy and single cell
120 tracking via time lapse analysis revealed remarkably high *oriC* and replisome
121 numbers during fast growth, suggesting multiple chromosomes and several
122 simultaneous replication events per cell. Initially cells possess two polar *oriC*-ParB
123 cluster, whereby upon replication sister *oriC*s segregate towards midcell positions.
124 Additionally, the length of replication periods as well as the overall DNA content was
125 determined for different growth conditions by marker-frequency analysis and flow
126 cytometry, thereby allowing the formulation of complete cell cycle models. Our data
127 suggest diploidy and overlapping C-periods in *C. glutamicum* and therefore, give new
128 insights in replication coordination within the group of actinobacteria.

129

130 **Materials and Methods**

131

132 **Oligonucleotides, plasmids and bacterial strains**

133 All primers, plasmids and bacterial strains used in this study are listed in Table S1
134 and S2, respectively.

135 **Strain construction**

136 Integration plasmids were constructed with 500 bp homologous regions upstream
137 and downstream of the 3' end of the gene to be labeled with a fluorophore sequence
138 in between. For pK19mobsacB-parB-eYFP and pK19mobsacB-parB-mCherry2
139 plasmids the upstream and downstream fragments were PCR amplified from the *C.*
140 *glutamicum* genome using the primer pairs ParB-Hind-up-F/ ParB-Sal-up-R and
141 ParB-XbaI-D-F/ ParB-Bam-D-R. eYFP or mCherry2 sequences were amplified using
142 primer pairs eYFP-SalI-F/ eYFP-XbaI-R or mCherry2-SalI-F/ mCherry2-XbaI-R. In

143 order to construct pK19mobsacB-DnaN-mCherry upstream and downstream
144 homologous regions were amplified via primer pairs DnaN-Hind-up-F/ DnaN-SphI-up-
145 R and DnaN-XbaI-D-F/ DnaN-BamHI-D-R. The mCherry sequence was amplified
146 using mCherry-SalI-F/ mCherry-XbaI-R primer pairs. The resulting PCR fragments
147 were digested with the respective restriction enzymes and consecutively ligated into
148 pK19mobsacB vectors. Plasmid cloning was performed using DH5α. *C. glutamicum*
149 were transformed via electroporation and selected for integration of the fluorophore
150 as described before (62). To confirm the allelic replacements *parB::parB-eYFP* and
151 *parB::parB-mCherry2* colony-PCR was carried out using primers ParB-N-ter-SalI-F
152 and ParB-PstI-800D-R and for the allelic replacement *dnaN::dnaN-mCherry* primers
153 DnaN-N-ter-F and DnaN-Bam-700D-R were used.

154 **Growth conditions and media**

155 *B. subtilis* and *E. coli* cells were grown in Luria-Bertani (LB) medium supplemented
156 with Kanamycin when appropriate at 37°C. *C. glutamicum* cells were grown in brain
157 heart infusion (BHI, Oxoid™) medium, BHI medium supplemented with 4% glucose
158 or in MMI medium (63) supplemented with 4% glucose, 120 mM acetate or 100 mM
159 propionate as indicated in the text at 30°C. For growth experiments in BHI
160 supplemented with glucose or MMI media cells were inoculated in BHI and diluted in
161 growth media overnight for pre-cultivation. The next morning cultures were diluted to
162 OD_{600} 1. Growth in BHI preceded an overnight inoculation step; cultures were re-
163 diluted to OD_{600} 0.5 the next morning. For replication runouts exponentially growing
164 *C. glutamicum* or *B. subtilis* cells were treated with 25 µg/ml or 200 µg/ml
165 chloramphenicol for 4+ h.

Fluorescence microscopy and life cell imaging

Fluorescence microscopy was carried out using an Axio-Imager M1 fluorescence microscope (Carl Zeiss) with an EC Plan Neofluar 100x/ 1.3 oil Ph3 objective and a 2.5 x optovar for automated image analysis. Filter sets 46 HE YFP (EX BP 500/25, BS FT 515, EM BP 535/30) and 43 HE Cy 3 shift free (EX BP 550/25, BS FT 570, EM BP 605/70) were used for fluorescence detection of eYFP and mCherry or mCherry2 protein fusions. DNA was stained using 1 µg/ml Hoechst 33342 (Thermo Scientific). For life cell imaging cells at exponential growth were re-diluted in BHI medium to OD_{600} 0.01 and loaded in a microfluidic chamber (B04A CellASIC®, Onix) at 8psi for 10 sec; for nutrient supply 0.75 psi were applied. Time lapse microscopy was performed using a Delta Vision Elite microscope (GE Healthcare, Applied Precision) with a standard four color InsightSSI module and an environmental chamber heated to 30°C. Images were taken with a 100×/ 1.4 oil PSF U-Plan S-Apo objective and mCherry (EX BP 575/25, EM BP 625/45) or YFP (EX BP 513/17, EM BP 548/22) specific filter sets were used for fluorescence detection (50% transmission, 0.3 sec exposure). Images were taken in 5 min intervals. For data analysis FIJI software (64) was applied; cell length measurements were acquired manually.

Marker frequency analysis

Genomic DNA was isolated from *C. glutamicum* or *B. subtilis* cells in exponential or stationary growth phases. DNA proximal to the origin or terminus (see text) was amplified by qPCR using a qPCR Mastermix (KAPA SYBR®FAST, Peqlab) according to manufacturer's protocol. Each experiment was performed in technical triplicates. Oligonucleotides used are listed in Table S1 and results were analyzed using the $2^{-\Delta CT}$ method (65).

Flow cytometry analysis

Culture samples were fixed 1:9 (v/v) in 70% ethanol and stored at 4°C until use. Cells were pelleted at 5000 rpm for 5 min and washed once in phosphate-buffered saline (PBS). The DNA staining procedure was adopted from a protocol described before (66). Samples were preheated to 37°C and stained in SYBR® Green I (Invitrogen) with a final dilution of 1:10000 for 15 min and consequently diluted in PBS. Flow cytometry analysis was performed using a BD Accuri C6 (BD Biosciences) with a 488 nm blue laser. The measurements were conducted at a flow rate of 10 µl/min with an acquisition threshold set to 700 on FL1-H and a rate of events per second less than 5000. At least 200000 events per sample were collected. Data were analyzed by plotting samples as histograms vs the green channel (FL1-A, EM BP 533/30) at log scale. All experiments were performed with biological triplicates.

In order to calibrate the DNA measurements of different growth conditions *B. subtilis* cells were used as an internal standard. A replication runout of *B. subtilis* cells grown in LB medium gave rise to cells with mainly 4 or 8 fully replicated chromosomes (67). Prior to ethanol fixation the cell wall was stained via strain-promoted alkyne-azide cycloaddition (SPAAC). In short 5 mM 3-azido-D-alanine (Baseclick GmbH), which incorporates into the cell wall, was added to the culture during the time of replication runout. Cells were washed in PBS, incubated with 10 µM DBCO-PEG_4-5/6-Carboxyrhodamine 110 (Jena Bioscience) at 30 °C for 20 min in the dark and subsequently washed three times in PBS + 0.1% Tween 80. This standard was included with *C. glutamicum* cells during incubation with 1 µg/ml Hoechst 33342 DNA stain. Flow cytometry was performed with a FACSAria II (Becton Dickinson) using a 488 nm blue laser and a 355 nm UV laser and appropriate filter sets. 50000 events were collected per sample. Blots of DNA content vs. the green channel were used to

identify *B. subtilis* subpopulations and *C. glutamicum* chromosome numbers were assessed in accordance with the standard in histograms vs. DNA amount.

For data analysis BD Accuri C6 software (BD Biosciences) or FlowJo software (Tree star, Inc.) were applied.

Analysis of the cell cycle

C- and D-periods were determined via equations relating to DNA amount per cell in exponential cultures (67,68), which were adapted to the *C. glutamicum* cell cycle model with double the number of chromosome equivalents at any time. Since only every second initiation is followed by a cell division the average *oriC*s per cell ($\bar{I}$) are defined as shown below. The term for the average *terC*s per cell ($\overline{T}$) was adjusted accordingly, where τ is the doubling time:

$$\bar{I} = 2 \times 2^{(C+D)/\tau}$$

$$\overline{T} = 2 \times 2^{D/\tau}$$

Hence, the D period was calculated as shown below; the average number of *oriC*s (I) per cell (N) was resolved by flow cytometry:

$$D = \frac{ln\left(\frac{I}{2}/N \times\right) \times T_d}{ln(2)} - C$$

The equation for determination of C periods does not change upon assumptions made above, where the *oriC* to *terC* ratio (I/T) was determined by marker frequency analysis:

$$C = \frac{ln(I/T) \times T_d}{ln(2)}$$

Statistical analysis

ANOVA and post hoc tests were performed using R (69); correlation coefficients, ANCOVA and linear regressions were calculated using Excel and Graph Pad Prism (GraphPad Software).

Results

Origin numbers correlate with cell length in a ParA-independent way.

We have shown before that the *C. glutamicum* partitioning protein ParB localizes at the origin regions of the chromosome close to the cell poles (51). However, in depth studies of spatiotemporal chromosome organization were still missing. Therefore, we aimed to reanalyze *oriC*-ParB complexes microscopically by time resolved life cell imaging. In order to label origin regions the native chromosomal *parB* locus of *C. glutamicum* RES167 wild type (WT) or in a Δ*parA* mutant was replaced by *parB-eYFP*, resulting in strains with typical cell morphology and growth phenotypes (Fig. 2A, Fig. S1). No cleavage products of ParB-eYFP were detectable (Fig. S2), suggesting that fluorescent signals faithfully reflect ParB localization. Microscopic analysis revealed a correlation of ParB-eYFP foci numbers with cell length in both strains (Fig. 2B). In the WT background between one and five foci were detected. The *parA* deletion mutant has variable cell lengths and anucleate minicells (not taken into account) were observed. Up to twelve ParB foci were present in cells of the *parA* deletion mutant. Notably, most of the ParB foci in the *parA* knockout strain were less fluorescent compared to the situation in wild type cells, suggesting that lack of ParA causes problems in the ParB assembly at the origin. Chromosome segregation

256 defects upon *parA* deletion do not markedly affect the high correlation of *oriC*-ParB
257 foci number to cell length. However, since linear regression models yield significant
258 differences between WT and the *parA* deletion strain (Fig. 2B) a loss of ParA might
259 cause slight over-initiation of chromosome replication.

260 In order to determine the maximal number of origins per cell precisely, an additional
261 allelic replacement of *divIVA* by *divIVA-mCherry* was carried out (Fig. 2C). With this
262 construct cell division can be monitored by DivIVA localization before the cells walls
263 of the daughter cells are separated, because DivIVA efficiently accumulates at the
264 septal membrane. This strain revealed WT-like growth rates and cell length
265 distributions (Fig. S1), suggesting that DivIVA-mCherry and ParB-eYFP are
266 functional. DivIVA localizes to the cell poles as well as newly formed septa and
267 therefore, is a suitable marker for completed cell division (60). Analysis revealed an
268 average of four ParB foci prior to completed septation at an average cell length of
269 3.94 µm, however, up to six foci per cell could be determined (Fig. 2D). Newborn
270 cells with an average length of 2.01 µm mostly contained 2 foci. Origin numbers and
271 cell size were relatively variable, as division septa are often not precisely placed at
272 midcell in *Corynebacteria*. Using the DivIVA reporter to judge ParB foci number per
273 daughter cell resulted in similar origin numbers per cell compared to using physical
274 separation of daughter cells as a mark for cell division. Notably these analyses
275 revealed unexpectedly high *oriC*-ParB cluster numbers that hint to the ability of *C.*
276 *glutamicum* to either undergo multifork replication and/or to harbor multiple fully
277 replicated chromosomes per cell.

278 **Spatiotemporal localization pattern of ParB-origin complexes.**

279 For analysis of chromosome arrangement during one cell cycle, life cell imaging was
280 performed using strain *C. glutamicum parB::parB-eYFP* (Fig. 3A, Movie S2). Single

cells with two ParB cluster were tracked over one generation time and foci positions were determined relative to the new pole, revealing distinct origin localization patterns throughout the cell cycle (Fig. 3B). New born cells contain two ParB foci stably located close to the cell poles. Newly replicated origins segregate from cell poles towards midcell. Often we observed the appearance of a new ParB cluster at either the new or old pole before a forth focus separates from the opposite ParB spot. No bias in timing of origin replication and segregation between old and new cell pole could be detected, as indicated by mean localizations of the third up to the fifth focus appearing around mid-cell positions. A timeline over one generation cycle shows the continuous increase of newly formed segregating origins (Fig. 3C). Already after completion of half a cell cycle (~30 min) around half of the cells contained four or five ParB foci; this ratio further increased during growth progression. In order to corroborate these findings we used automated analysis of still microscopy images to confirm the spatiotemporal *oriC*-ParB cluster localization (Fig 3D). Therefore, we programmed a Fiji software plug-in termed Morpholyzer that allows automated cell detection and analysis of fluorescent profiles (see material an methods). High ParB fluorescence intensities were detected close to the poles for all cells measured, suggesting stable origin anchoring at the cell poles. Segregation of sister *oriC*-ParB cluster towards midcell positions could be detected after around one fourth of the cell cycle (Fig. 3D). Similar dynamics of origin localization and segregation patterns have been characterized before for *M. xanthus*, *C. crescentus*, *M. smegmatis* and *V. cholera* (33,70-73). Upon ParA deletion the time dependent increase of origin numbers became less distinct due to large cell length variations directly after cytokinesis (Fig. 3E). As a consequence, already in large newborn cells multiple *oriC*-ParB complexes were present. Analysis of still images further revealed a disrupted ParB-origin pattern in *parA* deletion strains compared to the coordinated cellular

origin movement in WT cells (Fig. 3F). Fluorescent foci were detected all along the longitudinal cell axis without clear sites of preference, underlining the crucial role of the partitioning protein ParA in polar and septal positioning of *oriC*-ParB cluster in *C. glutamicum*.

Uniform timing of replication initiation at old and young cell poles.

C. glutamicum cells grow asymmetric by unequal rates of peptidoglycan-synthesis (PG) at the cell poles. The old cell pole synthesizes more PG compared to the young pole (74) due to cell cycle dependent dynamics of DivIVA accumulation (own unpublished data). As *C. glutamicum* DivIVA interacts with the origin-attached ParB protein (60) an impact of the DivIVA level on chromosome replication or segregation timing was investigated. Using automated analysis of cells co-expressing ParB-eYFP and DivIVA-mCherry old cell poles were identified by higher DivIVA fluorescence intensities and aligned accordingly. The fluorescence profile visualized in Figure 3G reveals synchronous origin movements towards the newly formed septum from both old and new cell poles, as suggested before by time-lapse analysis (Fig. 3B). Therefore, timing of chromosome replication seems to be uncoupled from the assembly of the cell wall synthesis machinery despite ParB-DivIVA interaction.

Replisome tracking reveals multiple replication forks and variable origin cohesion times.

In vivo characterization of replisome dynamics was carried out using a reporter strain in which the native locus of helicase sliding clamp *dnaN* was replaced by a *dnaN-mCherry* fusion construct (Fig. 4A). Cell length distribution and growth of the DnaN-mCherry expressing strain resembles the WT situation (Fig. S1) and the presence of full-length DnaN-mCherry protein could be confirmed via western blot (S2), suggesting that the localization patterns are not due to free fluorophores or degraded

protein. In order to track the pattern of replication timing automated analysis of fluorescence microscopy images was applied on cells grown in BHI (Fig. 4B). In growing cells high DnaN-mCherry signals were observed in a wide range around midcell. At the end of the first third of the generation time a fluent transition of replication termination around midcell towards formation of newly formed replication hubs in cell quarter positions took place. This large scale microscopy analysis clearly indicates that new rounds of replication initiation cannot be temporally separated from the previous ones. C-periods follow each other at short intervals or might even overlap during fast growth conditions. Notably, single cell analysis can show that replisomes are formed at polar or septal *oriC*-ParB complexes and gradually move away from the origins towards midcell (Fig. S3). Such a DnaN fluorescence pattern is not immediately obvious in kymographs, presumably due to variable timing of replication initiation between cells of similar size. The movement of replication forks observed by life cell imaging appeared to be highly dynamic (Movie S2). During life cell imaging a progressive increase of DnaN-foci over one generation time was observed (Fig. 4C). Initially two replication forks were counted for most of the cells; the number further increased to up to six foci per cell throughout the cell cycle indicating three or more simultaneous replication events per cell. In order to further analyze replication initiation and progression in dependence of origin localization a dual-reporter strain expressing ParB-eYFP and DnaN-mCherry was constructed. WT-like growth and cell lengths for this strain were confirmed (Fig. S1). The dependence of ParB-eYFP and DnaN-mCherry foci numbers on cell length is shown in Figure 4D. On average less DnaN than ParB spots were counted per cell, as indicated by regression lines. However, the replication fork number could have been underestimated due to frequent merging of forks initiated from the same origin. These results reveal simultaneous replication events of several chromosome equivalents

per cell. Furthermore, a moderate correlation between number of *oriC*-ParB clusters and replication forks per cell could be determined. Using life cell imaging cohesion periods of sister origins were analyzed, which are defined as the time between the formation of a new DnaN-mCherry spot in colocalization with an *oriC*-ParB cluster and the subsequent splitting of the latter into two distinct fluorescent signals (Fig. 4E). Time frames between replication initiation and sister origin segregation are illustrated in Figure 4F, revealing cohesion periods measured between 5 up to 80 min with an average of 36 min. The mean interval length is comparable to the 40 min origin colocalization period in fast growing *E. coli* cells determined before (75). As origin colocalization periods appear to be highly variable, a tight regulation for their cohesion might be absent in this organism. Replication initiations in the mother generation could frequently be observed with origin splitting only in subsequent generations as exemplified in Figure 4F. Notably, new rounds of chromosome replication were initiated at polar as well as at midcell positioned origins (Fig. S3).

Overlapping replication periods allow for fast growth.

The observation of multiple DnaN and ParB foci suggest the possibility that *C. glutamicum* is able to initiate new replication rounds before finishing the ongoing replication. To test this hypothesis, we applied marker frequency analysis to investigate growth rate dependent replication patterns of *C. glutamicum*. *OriC*/*ter* ratios were determined for cells grown in three different media (BHI, BHI+Gluc or MMI) allowing for fast, intermediate or slow growth (Fig. S4A). Data from qPCR experiments using markers of origin and terminus proximal regions prove a growth rate dependency of *oriC*/*ter* ratios (Fig. 5A). As control we analyzed *B. subtilis* cells an organism with clear multi-fork replication. Exponentially grown *B. subtilis* cells result in *oriC*/*ter* ratios considerably above of 2 (Fig. S4C). Analysis of exponentially

383 growing *C. glutamicum* cells cultured in BHI and BHI medium supplemented with
384 glucose yielded mean *oriC*/*ter* ratios of 2.4 and 2.2, indicating an overlap of
385 replication periods. Under slow growth conditions in MMI medium the mean *oriC/ter*
386 ratio of 1.7 did not significantly differ from values obtained from cells in stationary
387 growth phases. Upon antibiotic treatment leading to replication run-outs (by inhibiting
388 replication initiation yielding fully replicated chromosomes) the ratios dropped to
389 values close to one (data not shown). These results were further supported by whole
390 genome sequencing of cells grown in BHI and MMI medium (Fig. 5B). Sequencing
391 coverages revealed a symmetric progression of replication forks on both arms of the
392 chromosome for all conditions tested. During exponential growth in BHI the mean
393 coverage of origin regions was around 2.1 fold the one measured for terminus
394 proximal regions. The *oriC*/*ter* ratio dropped to 1.5 for log-phase cells grown in MMI
395 medium as well as for cells of stationary growth phases. These results hint to a
396 fraction of cells, which did not complete replication at stationary growth. Likewise,
397 active replication forks were observed in around 24 % of stationary *M. smegmatis*
398 cells (73). Marker frequency analysis and genome sequencing results point to growth
399 rate dependent replication cycles in *C. glutamicum* cells, where the timing of a new
400 initiation precedes termination of the previous replication event in order to enable fast
401 growth.

402 **_C. glutamicum_ cells contain multiple chromosome equivalents at varying**
403 **growth rates.**

404 As shown by marker frequency analysis *oriC*/*ter* ratios are considerably higher in fast
405 growing compared to slow growing cells. In order to more precisely verify the DNA
406 content per cell flow cytometry was applied. To this end, replication run-out of WT
407 cells cultured at varying growth rates were performed and nucleoids were

fluorescently stained with SYBR® Green I dye. DNA histograms show the number of fully replicated chromosomes, which equal the cellular origin numbers at the time point of antibiotic treatment (Fig. 5C). Absolute DNA content was assigned according to an internal standard (Fig. S5). Fast and intermediate growth conditions gave rise to mainly four and eight chromosomes per cell and a smaller fraction of cells contained ten and twelve chromosomes. Slow growth conditions yielded mainly cells containing either two or four and a small subpopulation containing eight chromosomes. Our data result in an average chromosome number per cell of 5.90, 5.17 and 3.85 from highest to lowest growth rate, respectively. Strikingly, the number of chromosome equivalents determined by flow cytometry is considerably higher than expected from marker frequency results and monoploid cell fractions were absent for all growth conditions tested in exponential phases. Flow cytometry results are further supported by fluorescence microscopy analysis of WT *parB::parB-eYFP* cells cultivated at several different growth rates. Cells with less than two ParB-foci per cell were almost absent under all condition tested. In addition, ParB-origin cluster numbers could possibly be underestimated due to potential origin cohesion (Fig. S6). Thus, we conclude that *C. glutamicum* is at least diploid with two chromosomes attached via the centromeric *oriC*-ParB nucleoprotein complex to the cell poles. Overinitiation of DNA replication leads to multi-ploid cells under fast growth conditions.

Growth rate dependent cell cycle models.

Cell cycle parameters derived from marker frequency and flow cytometry analysis (Table 1) allowed us to formulate complete cell cycle models at different growth conditions for *C. glutamicum*. A C-period of 78 min was determined for cells grown in BHI medium, whereas intermediate and low growth rates are associated with slightly longer replication periods of 96 and 97 min. These values result in a DNA replication

433 speed of around 340 bases/ sec, which is in the range of replication speeds reported
434 for *C. crescentus*, *M. xanthus* or *M. smegmatis* (Table 2 and references therein). D-
435 period equations reported before (67) yielded time intervals longer than the doubling
436 time for each of the three growth conditions analyzed indicating the presence of two
437 fully replicated chromosomes per newborn cell. Since we define the D-period as time
438 interval from replication termination that took place in the current generation until
439 subsequent cell division D period calculation was adapted to a diploid organism (see
440 Material and Methods). Those timeframes remained relatively unaltered with 20, 18
441 and 26 min from fast to slow growth rates, respectively.

442 Growth rate dependent cell cycle modes are illustrated for fast and slow growth
443 conditions (Fig. 6). Newborn cells localize their origins in two clusters at polar
444 positions with chromosomes being arranged longitudinally. During cell cycle
445 progression sister *oriC*-ParB complexes segregate and move towards septal
446 positions, whereby up to 4 ParB foci in MMI and up to 6 ParB foci per cell could be
447 detected microscopically. Overlapping C-periods allow for short doubling times of
448 down to 63 min with a new round of replication initiating 28 min after cell division and
449 the ongoing replication event terminating 15 min later. Cells with long doubling times
450 of 130 min possess a short time interval of seven min between cell division and
451 replication initiation (B-period) and fully replicate both chromosome copies once per
452 generation. In both, the fast and the slow growth model cells are diploid, since newly
453 replicated sister chromosomes will only be separated by cell division in the daughter
454 generation. Conclusively, cell cycle models suggested here describe overlapping
455 replication cycles in combination with two sets of chromosomes in *C. glutamicum*.

456

Discussion

The bacterial cell cycle has been analyzed in few model organisms in the past. A hallmark of fast growing species such as *E. coli*, *B. subtilis* is the initiation of new rounds of DNA replication prior to replication termination and cytokinesis (15,16). This process has been termed multi-fork replication. In slow growing species, or species with asymmetric division such as *C. crescentus* and *M. smegmatis* C-periods are not overlapping (13,14). The increasing knowledge about bacterial cell biology has made clear that even fundamental cell processes such as cytokinesis and DNA replication might be organized and regulated in a far higher diversity than initially thought (76,77). We have therefore analyzed the cell cycle in *C. glutamicum* under various growth conditions and different growth rates. *C. glutamicum* emerges as a model organism for apical cell growth that is characteristic for actinomycetales (61).

Analysis of ParB foci in growing *C. glutamicum* cells revealed that under all culture conditions a ParB focus is stably attached to each pole, suggesting an *ori-ter-ter-ori* orientation of the chromosomes (Fig. 2 & 3). Interestingly, newly replicated origins segregate to midcell were they remain until cytokinesis is completed and they stay tethered to the newly forming cell poles (Fig. 3). Up to now it is unclear by which molecular mechanism the placement of ParB and the chromosomal origin is directed. Earlier work has shown that ParB and the cell division protein FtsZ interact (51). Interaction of ParB with the divisome might be a plausible explanation for the observed localization pattern. Deletion of ParA completely abolishes the directed ParB segregation, confirming earlier results from our group (51). Thus, unlike in other species with polar origin localization, such as *C. crescentus* and *V. cholerae*, the newly replicated origin is not migrating to the opposite pole (32,78). This mode of segregation in *C. glutamicum* is compatible with the observation that both cell poles

482 are constantly occupied with a ParB-*oriC* complex, suggesting that even newborn
483 cells contain at least two chromosomes and, hence, are diploid. Due to variable
484 cohesion times of sister chromatids (Fig. 4C) the number of ParB foci does not
485 necessarily reflect the number of origins and may lead to an underestimation of
486 origins. The existence of several chromosomes is in line with the observation of
487 multiple replication forks. During replication two or more replication forks can be
488 visualized as judged by fluorescently labeled sliding clamp DnaN (Fig. 4).
489 Localization of origins in *C. glutamicum* is therefore different from the situation in the
490 closely related *M. smegmatis*. For *M. smegmatis* a replication factory model has been
491 proposed in which a central localized origin is replicated and the newly replicated
492 origins are segregated towards the cell pole while the replisome remains in the cell
493 center (72). In contrast, we show by time lapse analysis that replication forks
494 originate close to the cell pole and migrate towards midcell in *C. glutamicum* (Fig. 4E,
495 Fig. S3). Thus, this organism does not have a static replication factory and, hence, is
496 not consistent with the replication factory model proposed for *B. subtilis* (79). We also
497 observed that both origins initiate replication around the same time. Further support
498 for diploidy stems from flow cytometry data (Fig. 5). In replication run-out experiments
499 cells contain a minimum of two and up to twelve chromosomes, being a clear
500 indication of multiple initiation during fast growth conditions (growth rate above 0.6 h^{-1}
501). Although presence of multiple chromosomes per cell has been suggested before
502 (80), only single cell analysis unambiguously supports the diploidy of *C. glutamicum*
503 cells. The simultaneous presence of two polar chromosomes is in stark contrast to
504 findings recently reported for *Mycobacterium* species (72,73). Corynebacteria and
505 Mycobacteria are closely related and, hence, it comes as a surprise that cellular
506 organization of their chromosomes might be different. The constant diploidy of *C.*
507 *glutamicum* could be a consequence of their environmental life style. Many soil

508 bacteria have elaborated sophisticated methods to counteract various environmental
509 stresses such as desiccation, nutrient shortage or exposure to DNA damaging
510 agents. In fact, nucleic acids are prominent targets for desiccation induced damage
511 (81). Cells carrying two or more chromosome equivalents will increase the change for
512 correct DNA repair based on homologous recombination. In line with this hypothesis
513 survival rates of coryneform bacteria are known to be high under various stresses
514 including desiccation (82-84). Analyses of long-term preservations of microbial
515 ecosystems in permafrost demonstrate that Corynebacteria are dominating older
516 sediments (84).

517 In summary, we have provided detailed analyses of the cell cycle of *C. glutamicum* at
518 different growth rates (Fig. 6). Data presented here point to a unique and so far
519 undescribed cell cycle regulation with two polar attached chromosomes that
520 simultaneously initiate replication. At fast growth conditions new rounds of replication
521 can be initiated before the previous round is complete, similar to multi-fork replication.
522 In contrast to other bacteria with polar oriented chromosomes, such as chromosome I
523 from *V. cholerae* or *C. crescentus*, *C. glutamicum* cells contain two copies of the
524 chromosomes and segregate the newly replicated origins only to midcell. The
525 elucidation of the corynebacterial cell cycle is important to fully understand growth
526 behavior and homologous recombination in this medically and industrially relevant
527 genus.

528

529

530 **References**

531 1. Wang, X., Llopis, P.M. and Rudner, D.Z. (2013) Organization and segregation of bacterial
532 chromosomes. *Nat Rev Genet*, **14**, 191-203.

2. Quon, K.C., Yang, B., Domian, I.J., Shapiro, L. and Marczynski, G.T. (1998) Negative control of bacterial DNA replication by a cell cycle regulatory protein that binds at the chromosome origin. *Proceedings of the National Academy of Sciences of the United States of America*, **95**, 120-125.
3. McGrath, P.T., Iniesta, A.A., Ryan, K.R., Shapiro, L. and McAdams, H.H. (2006) A dynamically localized protease complex and a polar specificity factor control a cell cycle master regulator. *Cell*, **124**, 535-547.
4. Gorbatyuk, B. and Marczynski, G.T. (2005) Regulated degradation of chromosome replication proteins DnaA and CtrA in Caulobacter crescentus. *Molecular microbiology*, **55**, 1233-1245.
5. Lu, M., Campbell, J.L., Boye, E. and Kleckner, N. (1994) SeqA: a negative modulator of replication initiation in *E. coli*. *Cell*, **77**, 413-426.
6. Nievera, C., Torgue, J.J.C., Grimwade, J.E. and Leonard, A.C. (2006) SeqA blocking of DnaA-*oriC* interactions ensures staged assembly of the *E. coli* pre-RC. *Molecular cell*, **24**, 581-592.
7. Beattie, T.R. and Reyes-Lamothe, R. (2015) A Replisome's journey through the bacterial chromosome. *Frontiers in microbiology*, **6**, 562.
8. Katayama, T., Ozaki, S., Keyamura, K. and Fujimitsu, K. (2010) Regulation of the replication cycle: conserved and diverse regulatory systems for DnaA and *oriC*. *Nature reviews. Microbiology*, **8**, 163-170.
9. Blakely, G., May, G., McCulloch, R., Arciszewska, L.K., Burke, M., Lovett, S.T. and Sherratt, D.J. (1993) Two related recombinases are required for site-specific recombination at *dif* and *cer* in E. coli K12. *Cell*, **75**, 351-361.
10. Aussel, L., Barre, F.-X., Aroyo, M., Stasiak, A., Stasiak, A.Z. and Sherratt, D. (2002) FtsK is a DNA motor protein that activates chromosome dimer resolution by switching the catalytic state of the XerC and XerD recombinases. *Cell*, **108**, 195-205.
11. Lemon, K.P. and Grossman, A.D. (2000) Movement of replicating DNA through a stationary replisome. *Molecular cell*, **6**, 1321-1330.
12. Jensen, R.B., Wang, S.C. and Shapiro, L. (2001) A moving DNA replication factory in *Caulobacter crescentus*. *The EMBO journal*, **20**, 4952-4963.
13. Santi, I., Dhar, N., Bousbaine, D., Wakamoto, Y. and McKinney, J.D. (2013) Single-cell dynamics of the chromosome replication and cell division cycles in mycobacteria. *Nature communications*, **4**, 2470.
14. Marczynski, G.T. (1999) Chromosome methylation and measurement of faithful, once and only once per cell cycle chromosome replication in *Caulobacter crescentus*. *Journal of bacteriology*, **181**, 1984-1993.
15. Cooper, S. and Helmstetter, C.E. (1968) Chromosome replication and the division cycle of *Escherichia coli* B/r. *Journal of molecular biology*, **31**, 519-540.
16. Quinn, W.G. and Sueoka, N. (1970) Symmetric replication of the *Bacillus subtilis* chromosome. *Proceedings of the National Academy of Sciences of the United States of America*, **67**, 717-723.
17. Stokke, C., Waldminghaus, T. and Skarstad, K. (2011) Replication patterns and organization of replication forks in *Vibrio cholerae*. *Microbiology*, **157**, 695-708.
18. Wang, J.D. and Levin, P.A. (2009) Metabolism, cell growth and the bacterial cell cycle. *Nat Rev Micro*, **7**, 822-827.
19. Soppa, J. (2014) Polyploidy in archaea and bacteria: about desiccation resistance, giant cell size, long-term survival, enforcement by a eukaryotic host and additional aspects. *Journal of Molecular Microbiology and Biotechnology*, **24**, 409-419.
20. Mendell, J.E., Clements, K.D., Choat, J.H. and Angert, E.R. (2008) Extreme polyploidy in a large bacterium. *Proceedings of the National Academy of Sciences*, **105**, 6730-6734.
21. Sadoff, H.L., Shimel, B. and Ellis, S. (1979) Characterization of *Azotobacter vinelandii* deoxyribonucleic acid and folded chromosomes. *Journal of bacteriology*, **138**, 871-877.
22. Nagpal, P., Jafri, S., Reddy, M.A. and Das, H.K. (1989) Multiple chromosomes of *Azotobacter vinelandii*. *Journal of bacteriology*, **171**, 3133-3138.

23. Pecoraro, V., Zerulla, K., Lange, C. and Soppa, J. (2011) Quantification of ploidy in proteobacteria revealed the existence of monoploid, (mero-)oligoploid and polyploid species. *PloS one*, **6**, e16392.
24. Hansen, M.T. (1978) Multiplicity of genome equivalents in the radiation-resistant bacterium *Micrococcus radiodurans*. *Journal of bacteriology*, **134**, 71-75.
25. Griese, M., Lange, C. and Soppa, J. (2011) Ploidy in cyanobacteria. *FEMS microbiology letters*, **323**, 124-131.
26. Hildenbrand, C., Stock, T., Lange, C., Rother, M. and Soppa, J. (2011) Genome copy numbers and gene conversion in methanogenic archaea. *Journal of bacteriology*, **193**, 734-743.
27. Michelsen, O., Hansen, F.G., Albrechtsen, B. and Jensen, P.R. (2010) The MG1363 and IL1403 laboratory strains of *Lactococcus lactis* and several dairy strains are diploid. *Journal of bacteriology*, **192**, 1058-1065.
28. Wang, X., Liu, X., Possoz, C. and Sherratt, D.J. (2006) The two *Escherichia coli* chromosome arms locate to separate cell halves. *Genes & development*, **20**, 1727-1731.
29. Bates, D. and Kleckner, N. (2005) Chromosome and replisome dynamics in *E. coli*: loss of sister cohesion triggers global chromosome movement and mediates chromosome segregation. *Cell*, **121**, 899-911.
30. Adachi, S., Kohiyama, M., Onogi, T. and Hiraga, S. (2005) Localization of replication forks in wild-type and *mukB* mutant cells of *Escherichia coli*. *Molecular Genetics and Genomics*, **274**, 264-271.
31. Viollier, P.H., Thanbichler, M., McGrath, P.T., West, L., Meewan, M., McAdams, H.H. and Shapiro, L. (2004) Rapid and sequential movement of individual chromosomal loci to specific subcellular locations during bacterial DNA replication. *Proceedings of the National Academy of Sciences of the United States of America*, **101**, 9257-9262.
32. Fogel, M.A. and Waldor, M.K. (2005) Distinct segregation dynamics of the two *Vibrio cholerae* chromosomes. *Molecular microbiology*, **55**, 125-136.
33. Fogel, M.A. and Waldor, M.K. (2006) A dynamic, mitotic-like mechanism for bacterial chromosome segregation. *Genes & development*, **20**, 3269-3282.
34. Vallet-Gely, I. and Boccard, F. (2013) Chromosomal organization and segregation in *Pseudomonas aeruginosa*. *PLoS genetics*, **9**, e1003492.
35. Bowman, G.R., Comolli, L.R., Zhu, J., Eckart, M., Koenig, M., Downing, K.H., Moerner, W.E., Earnest, T. and Shapiro, L. (2008) A polymeric protein anchors the chromosomal origin/ParB complex at a bacterial cell pole. *Cell*, **134**, 945-955.
36. Yamaichi, Y., Bruckner, R., Ringgaard, S., Möll, A., Cameron, D.E., Briegel, A., Jensen, G.J., Davis, B.M. and Waldor, M.K. (2012) A multidomain hub anchors the chromosome segregation and chemotactic machinery to the bacterial pole. *Genes & development*, **26**, 2348-2360.
37. Wang, X., Montero Llopis, P. and Rudner, D.Z. (2014) *Bacillus subtilis* chromosome organization oscillates between two distinct patterns. *Proceedings of the National Academy of Sciences*, **111**, 12877-12882.
38. Livny, J., Yamaichi, Y. and Waldor, M.K. (2007) Distribution of centromere-like *parS* sites in bacteria: insights from comparative genomics. *Journal of bacteriology*, **189**, 8693-8703.
39. Kiekebusch, D. and Thanbichler, M. (2014) Plasmid segregation by a moving ATPase gradient. *Proceedings of the National Academy of Sciences of the United States of America*, **111**, 4741-4742.
40. Lin, D.C. and Grossman, A.D. (1998) Identification and characterization of a bacterial chromosome partitioning site. *Cell*, **92**, 675-685.
41. Murray, H., Ferreira, H. and Errington, J. (2006) The bacterial chromosome segregation protein Spo0J spreads along DNA from *parS* nucleation sites. *Molecular microbiology*, **61**, 1352-1361.

42. Breier, A.M. and Grossman, A.D. (2007) Whole-genome analysis of the chromosome partitioning and sporulation protein Spo0J (ParB) reveals spreading and origin-distal sites on the *Bacillus subtilis* chromosome. *Molecular microbiology*, **64**, 703-718.
43. Graham, T.G.W., Wang, X., Song, D., Etson, C.M., van Oijen, A.M., Rudner, D.Z. and Loparo, J.J. (2014) ParB spreading requires DNA bridging. *Genes & development*, **28**, 1228-1238.
44. Leonard, T.A., Butler, P.J. and Löwe, J. (2005) Bacterial chromosome segregation: structure and DNA binding of the Soj dimer – a conserved biological switch. *The EMBO journal*, **24**, 270-282.
45. Ptacin, J.L., Lee, S.F., Garner, E.C., Toro, E., Eckart, M., Comolli, L.R., Moerner, W.E. and Shapiro, L. (2010) A spindle-like apparatus guides bacterial chromosome segregation. *Nat Cell Biol*, **12**, 791-798.
46. Iniesta, A.A. (2014) ParABS system in chromosome partitioning in the bacterium *Myxococcus xanthus*. *PloS one*, **9**, e86897.
47. Lim, H.C., Surovtsev, I.V., Beltran, B.G., Huang, F., Bewersdorf, J. and Jacobs-Wagner, C. (2014) Evidence for a DNA-relay mechanism in ParABS-mediated chromosome segregation. *eLife*, **3**, e02758.
48. Hwang, L.C., Vecchiarelli, A.G., Han, Y.W., Mizuuchi, M., Harada, Y., Funnell, B.E. and Mizuuchi, K. (2013) ParA-mediated plasmid partition driven by protein pattern self-organization. *The EMBO journal*, **32**, 1238-1249.
49. Vecchiarelli, A.G., Hwang, L.C. and Mizuuchi, K. (2013) Cell-free study of F plasmid partition provides evidence for cargo transport by a diffusion-ratchet mechanism. *Proceedings of the National Academy of Sciences of the United States of America*, **110**, E1390-1397.
50. Lewis, R.A., Bignell, C.R., Zeng, W., Jones, A.C. and Thomas, C.M. (2002) Chromosome loss from par mutants of *Pseudomonas putida* depends on growth medium and phase of growth. *Microbiology*, **148**, 537-548.
51. Donovan, C., Schwaiger, A., Krämer, R. and Bramkamp, M. (2010) Subcellular localization and characterization of the ParAB system from *Corynebacterium glutamicum*. *Journal of bacteriology*, **192**, 3441-3451.
52. Jakimowicz, D., Brzostek, A., Rumijowska-Galewicz, A., Żydek, P., Dołzbłasz, A., Smulczyk-Krawczyszyn, A., Zimniak, T., Wojtasz, Ł., Zawilak-Pawlik, A., Kois, A. *et al.* (2007) Characterization of the mycobacterial chromosome segregation protein ParB and identification of its target in *Mycobacterium smegmatis*. *Microbiology*, **153**, 4050-4060.
53. Ireton, K., Gunther, N.W. and Grossman, A.D. (1994) spo0J is required for normal chromosome segregation as well as the initiation of sporulation in *Bacillus subtilis*. *Journal of bacteriology*, **176**, 5320-5329.
54. Ginda, K., Bezulska, M., Ziolkiewicz, M., Dziadek, J., Zakrzewska-Czerwinska, J. and Jakimowicz, D. (2013) ParA of *Mycobacterium smegmatis* co-ordinates chromosome segregation with the cell cycle and interacts with the polar growth determinant DivIVA. *Molecular microbiology*, **87**, 998-1012.
55. Mohl, D.A., Easter, J., Jr. and Gober, J.W. (2001) The chromosome partitioning protein, ParB, is required for cytokinesis in *Caulobacter crescentus*. *Molecular microbiology*, **42**, 741-755.
56. Charaka, V.K. and Misra, H.S. (2012) Functional characterization of the role of the chromosome I partitioning system in genome segregation in *Deinococcus radiodurans*. *Journal of bacteriology*, **194**, 5739-5748.
57. WHO. (2016). Wold health organization, Geneva, www.who.int/tb/publications/global_report/en/ (accessed Nov 04, 2016).
58. Wendisch, V.F., Jorge, J.M., Pérez-García, F. and Sgobba, E. (2016) Updates on industrial production of amino acids using *Corynebacterium glutamicum*. *World journal of microbiology & biotechnology*, **32**, 105.
59. Donovan, C., Schauss, A., Krämer, R. and Bramkamp, M. (2013) Chromosome segregation impacts on cell growth and division site selection in *Corynebacterium glutamicum*. *PloS one*, **8**, e55078.

60. Donovan, C., Sieger, B., Krämer, R. and Bramkamp, M. (2012) A synthetic *Escherichia coli* system identifies a conserved origin tethering factor in Actinobacteria. *Molecular microbiology*, **84**, 105-116.
61. Donovan, C. and Bramkamp, M. (2014) Cell division in *Corynebacterineae*. *Frontiers in microbiology*, **5**, 132.
62. Schäfer, A., Tauch, A., Jäger, W., Kalinowski, J., Thierbach, G. and Pühler, A. (1994) Small mobilizable multi-purpose cloning vectors derived from the *Escherichia coli* plasmids pK18 and pK19: selection of defined deletions in the chromosome of *Corynebacterium glutamicum*. *Gene*, **145**, 69-73.
63. Nottebrock, D., Meyer, U., Krämer, R. and Morbach, S. (2003) Molecular and biochemical characterization of mechanosensitive channels in *Corynebacterium glutamicum*. *FEMS microbiology letters*, **218**, 305-309.
64. Schindelin, J., Arganda-Carreras, I., Frise, E., Kaynig, V., Longair, M., Pietzsch, T., Preibisch, S., Rueden, C., Saalfeld, S., Schmid, B. *et al.* (2012) Fiji: an open-source platform for biological-image analysis. *Nat Meth*, **9**, 676-682.
65. Livak, K.J. and Schmittgen, T.D. (2001) Analysis of relative gene expression data using real-time quantitative PCR and the 2(-Delta Delta C(T)) Method. *Methods*, **25**, 402-408.
66. Hammes, F., Berney, M., Wang, Y., Vital, M., Köster, O. and Egli, T. (2008) Flow-cytometric total bacterial cell counts as a descriptive microbiological parameter for drinking water treatment processes. *Water research*, **42**, 269-277.
67. Hill, N.S., Kadoya, R., Chattoraj, D.K. and Levin, P.A. (2012) Cell Size and the Initiation of DNA Replication in Bacteria. *PLoS genetics*, **8**, e1002549.
68. Bremer, H. and Churchward, G. (1977) An examination of the Cooper-Helmstetter theory of DNA replication in bacteria and its underlying assumptions. *Journal of theoretical biology*, **69**, 645-654.
69. Team, R.C. (2014). URL http://www.R-project.org/.
70. Harms, A., Treuner-Lange, A., Schumacher, D. and Søgaard-Andersen, L. (2013) Tracking of chromosome and replisome dynamics in *Myxococcus xanthus* reveals a novel chromosome arrangement. *PLoS genetics*, **9**, e1003802.
71. Thanbichler, M. and Shapiro, L. (2006) MipZ, a spatial regulator coordinating chromosome segregation with cell division in *Caulobacter*. *Cell*, **126**, 147-162.
72. Santi, I. and McKinney, J.D. (2015) Chromosome organization and replisome dynamics in *Mycobacterium smegmatis*. *mBio*, **6**.
73. Trojanowski, D., Ginda, K., Pióro, M., Hołówka, J., Skut, P., Jakimowicz, D. and Zakrzewska-Czerwińska, J. (2015) Choreography of the *Mycobacterium* replication machinery during the cell cycle. *mBio*, **6**.
74. Sieger, B., Schubert, K., Donovan, C. and Bramkamp, M. (2013) The lipid II flippase RodA determines morphology and growth in *Corynebacterium glutamicum*. *Molecular microbiology*, **90**, 966-982.
75. Fossum, S., Crooke, E. and Skarstad, K. (2007) Organization of sister origins and replisomes during multifork DNA replication in *Escherichia coli*. *The EMBO journal*, **26**, 4514-4522.
76. Badrinarayanan, A., Le, T.B. and Laub, M.T. (2015) Bacterial chromosome organization and segregation. *Annual review of cell and developmental biology*, **31**, 171-199.
77. Randich, A.M. and Brun, Y.V. (2015) Molecular mechanisms for the evolution of bacterial morphologies and growth modes. *Frontiers in microbiology*, **6**, 580.
78. Jensen, R.B. and Shapiro, L. (1999) The *Caulobacter crescentus smc* gene is required for cell cycle progression and chromosome segregation. *Proceedings of the National Academy of Sciences of the United States of America*, **96**, 10661-10666.
79. Lemon, K.P. and Grossman, A.D. (1998) Localization of bacterial DNA polymerase: evidence for a factory model of replication. *Science*, **282**, 1516-1519.

80. Neumeyer, A., Hübschmann, T., Müller, S. and Frunzke, J. (2013) Monitoring of population dynamics of *Corynebacterium glutamicum* by multiparameter flow cytometry. *Microbial biotechnology*, **6**, 157-167.
81. Potts, M. (1994) Desiccation tolerance of prokaryotes. *Microbiological reviews*, **58**, 755-805.
82. Ochrombel, I., Ott, L., Krämer, R., Burkovski, A. and Marin, K. (2011) Impact of improved potassium accumulation on pH homeostasis, membrane potential adjustment and survival of *Corynebacterium glutamicum*. *Biochimica et biophysica acta*, **1807**, 444-450.
83. Miyamoto-Shinohara, Y., Sukenobe, J., Imaizumi, T. and Nakahara, T. (2008) Survival of freeze-dried bacteria. *The Journal of general and applied microbiology*, **54**, 9-24.
84. Gilichinsky, D.A., Vorobyova, E.A., Erokhina, L.G., Fyordorov-Davydov, D.G., Chaikovskaya, N.R. and Fyordorov-Dayvdov, D.G. (1992) Long-term preservation of microbial ecosystems in permafrost. *Advances in space research : the official journal of the Committee on Space Research*, **12**, 255-263.
85. Nair, N., Dziedzic, R., Greendyke, R., Muniruzzaman, S., Rajagopalan, M. and Madiraju, M.V. (2009) Synchronous replication initiation in novel *Mycobacterium tuberculosis dnaA* cold-sensitive mutants. *Molecular microbiology*, **71**, 291-304.
86. Zusman, D. and Rosenberg, E. (1970) DNA cycle of *Myxococcus xanthus*. *Journal of molecular biology*, **49**, 609-619.
87. Dingwall, A. and Shapiro, L. (1989) Rate, origin, and bidirectionality of *Caulobacter* chromosome replication as determined by pulsed-field gel electrophoresis. *Proceedings of the National Academy of Sciences of the United States of America*, **86**, 119-123.
88. Rasmussen, T., Jensen, R.B. and Skovgaard, O. (2007) The two chromosomes of *Vibrio cholerae* are initiated at different time points in the cell cycle. *The EMBO journal*, **26**, 3124-3131.
89. Sharpe, M.E., Hauser, P.M., Sharpe, R.G. and Errington, J. (1998) *Bacillus subtilis* cell cycle as studied by fluorescence microscopy: constancy of cell length at initiation of DNA replication and evidence for active nucleoid partitioning. *Journal of bacteriology*, **180**, 547-555.
90. Kubitschek, H.E. and Freedman, M.L. (1971) Chromosome replication and the division cycle of *Escherichia coli* B/r. *Journal of bacteriology*, **107**, 95-99.
91. Michelsen, O., Teixeira de Mattos, M.J., Jensen, P.R. and Hansen, F.G. (2003) Precise determinations of C and D periods by flow cytometry in *Escherichia coli* K-12 and B/r. *Microbiology*, **149**, 1001-1010.
92. Tanner, N.A., Loparo, J.J., Hamdan, S.M., Jergic, S., Dixon, N.E. and van Oijen, A.M. (2009) Real-time single-molecule observation of rolling-circle DNA replication. *Nucleic acids research*, **37**, e27.

Acknowledgements

The authors are thankful to Dr. Andreas Brachmann (LMU) for help with the genome sequencing. We thank Dr. Stephan Gruber (Max-Planck-Institute for Biochemistry) for stimulating discussions and suggestions. This work was funded by grants from the Deutsche Forschungsgemeinschaft (BR2815/6-1) and the Ministry of Science and Education (BMBF: 031A302 e:Bio-Modul II: 0.6 plus).

779

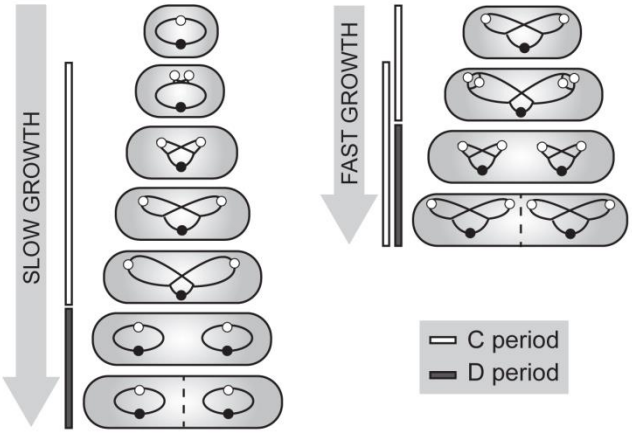

Figure 1. Schematic representation of bacterial replication cycles under slow (left) and fast (right) growth conditions.

During slow growth conditions DNA replication (termed C-period) takes place within a single generation, followed by the interval between replication termination and completion of cell division (D-period). Fast growing bacteria with generation times of less than the C period, like *Bacillus subtilis* and *Escherichia coli*, undergo multifork replication, i.e. new rounds of replication are initiated before previous ones terminate. Chromosomes are indicated by black lines with *oriCs* and *terCs* as white and black circles.

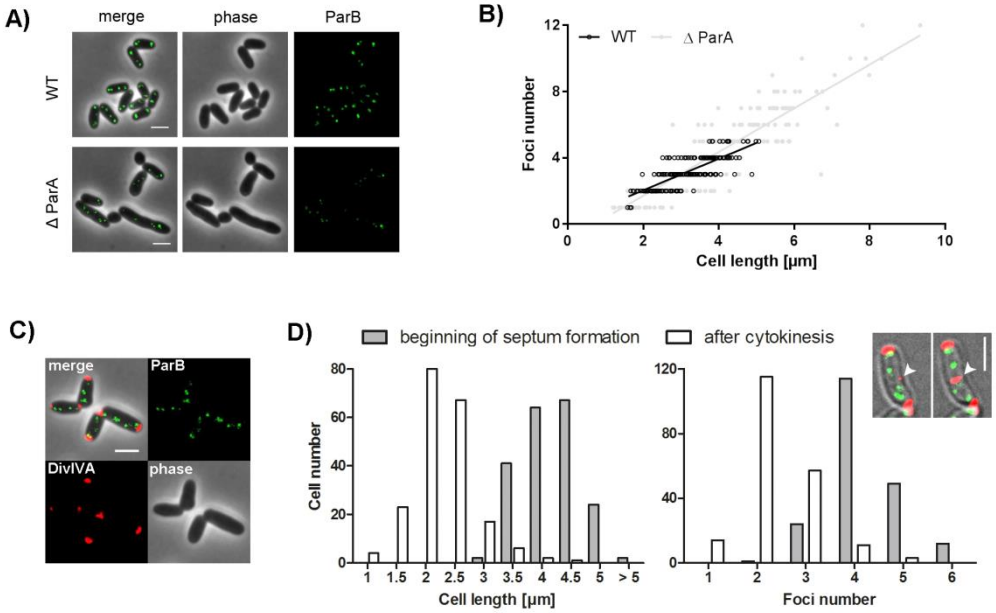

792

793 **Figure 2. Determination of the *C. glutamicum oriC* number and correlation to**

794 **cell length.**

795 **A)** Subcellular localization of ParB-eYFP in representative *parB::parB-eYFP* wild type

796 (WT) and Δ*parA* cells. Shown are overlays between phase contrast images and

797 eYFP fluorescence (merge) and separate channels (phase, ParB). Scale bar, 2 µm.

798 **B)** ParB foci number depend on cell length in a ParA independent way. In wild type

799 strain (WT) one to five foci and in Δ*parA* strain one to twelve foci were observed

800 (n=400). Linear regression lines are shown r(wild type)=0.80, r(Δ*parA*)=0.88; slopes

801 are not equal (ANCOVA, F(1, 396)=16.10, p <.0001). **C)** Still image of *C. glutamicum*

802 *parB::parB-eYFP divIVA::divIVA-mCherry* cells. Depicted are phase contrast (lower

803 right), DivIVA (lower left) and ParB-eYFP fluorescence (upper right) and the overlay

804 of all channels (upper left). Scale bar, 2 µm. **D)** Time-lapse microscopy of DivIVA-

805 mCherry and ParB-eYFP coexpressing strain reveals distribution of cell length and

806 ParB-eYFP cluster number at the beginning of septum formation and after cell

807 division (n=200). The microscopy images of a single cell exemplify the time lapse of

808 septum formation (white arrowhead) tracked by DivIVA-mCherry reporter. Scale bar,

809 2 µm.

810

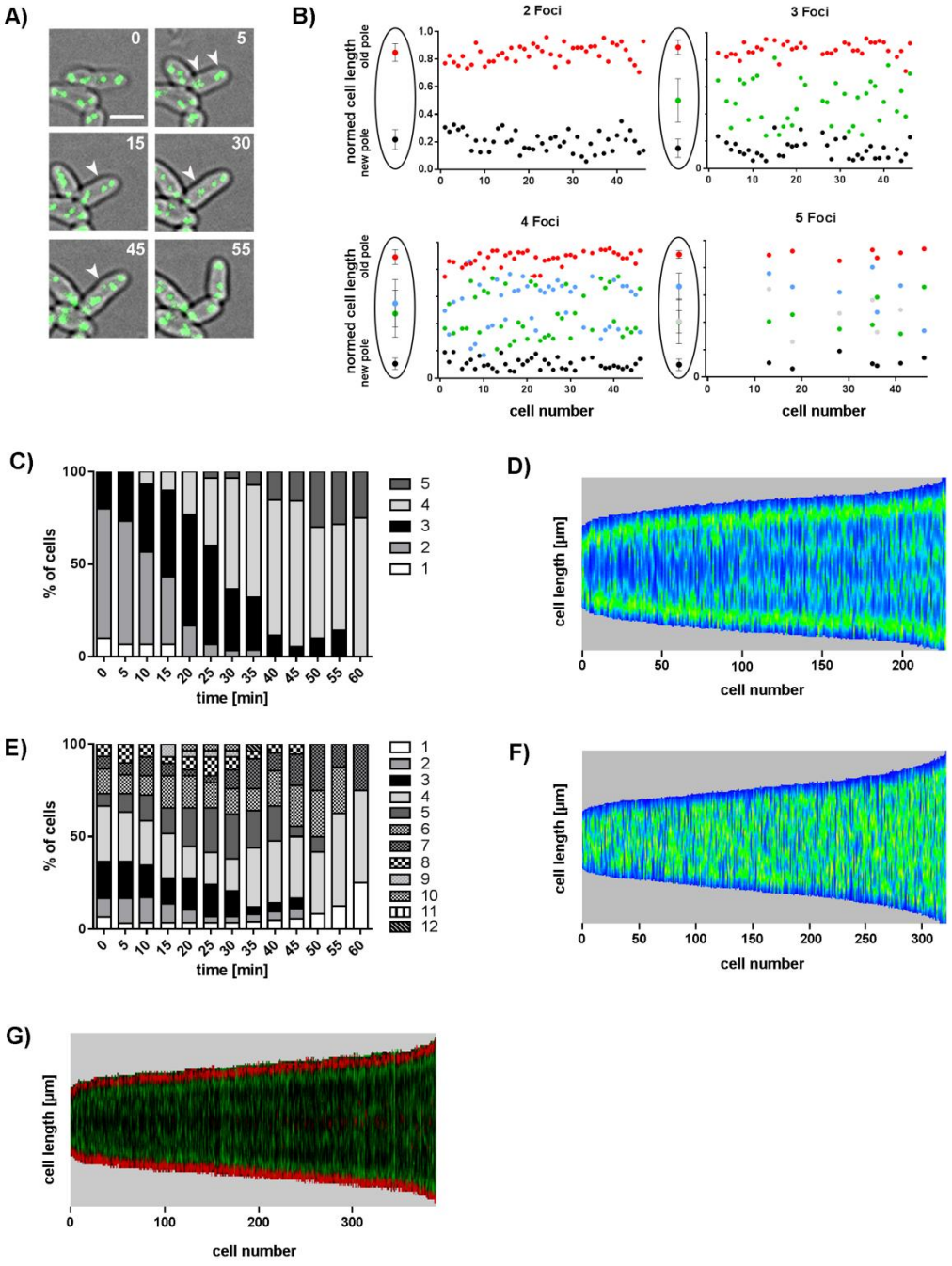

Figure 3. *OriC* localization pattern during cell cycle progression.

A) Occurrence of newly formed ParB-eYFP clusters in the course of cell elongation. Still images show a time series of a typical *C. glutamicum* wild type cell with initially two ParB spots. Three further foci appear over time (white arrowheads); time points are indicated in min (top right corner). Scale bar, 2 µm. **B)** Time lapse single cell

817 analyses reveal *oriC*-ParB complex positions along the long cell axis at each moment
818 in time a new ParB-eYFP spot occurs. A third, fourth and eventually a fifth focus
819 separate from the two initial ParB clusters located close to the cell poles and move
820 towards midcell positions. Cells are aligned with the old pole facing upwards; cell
821 lengths are normed to 1 (n=46). Schemes as shown to the left illustrate average
822 ParB-eYFP foci positions ± standard deviation. **C)** Time dependent increase of ParB
823 clusters per cell. Fraction of cells with 1-5 spots are depicted for each time point
824 (n=30). **D)** ParB-eYFP pattern along the cell axis in dependence of cell length in wild
825 type *C. glutamicum*. Automated image analysis of still microscopy images sorted by
826 cell length with high fluorescence intensities displayed in green (n>200). **E)** Counts of
827 ParB-eYFP spots over time in *C. glutamicum* Δ*parA*. Percentages of cells with 1-12
828 ParB foci were determined for each time point (n=30). **F)** Random ParB-eYFP
829 distribution along the longitudinal cell axis in relation to its length in Δ*parA* mutant
830 strain. Automated analysis of still images with high fluorescence intensities displayed
831 in green (n>300). **G)** Timing of replication initiation is similar at *oriC* of old and young
832 cell pole. Automated image analysis of *C. glutamicum parB::parB-eYFP*
833 *divIVA::divIVA-mCherry* fluorescence pattern sorted by cell length with the old cell
834 pole (high polar DivIVA-mCherry signal) facing downwards. ParB-eYFP (green) and
835 DivIVA-mCherry (red) fluorescence are illustrated in one kymograph.

836

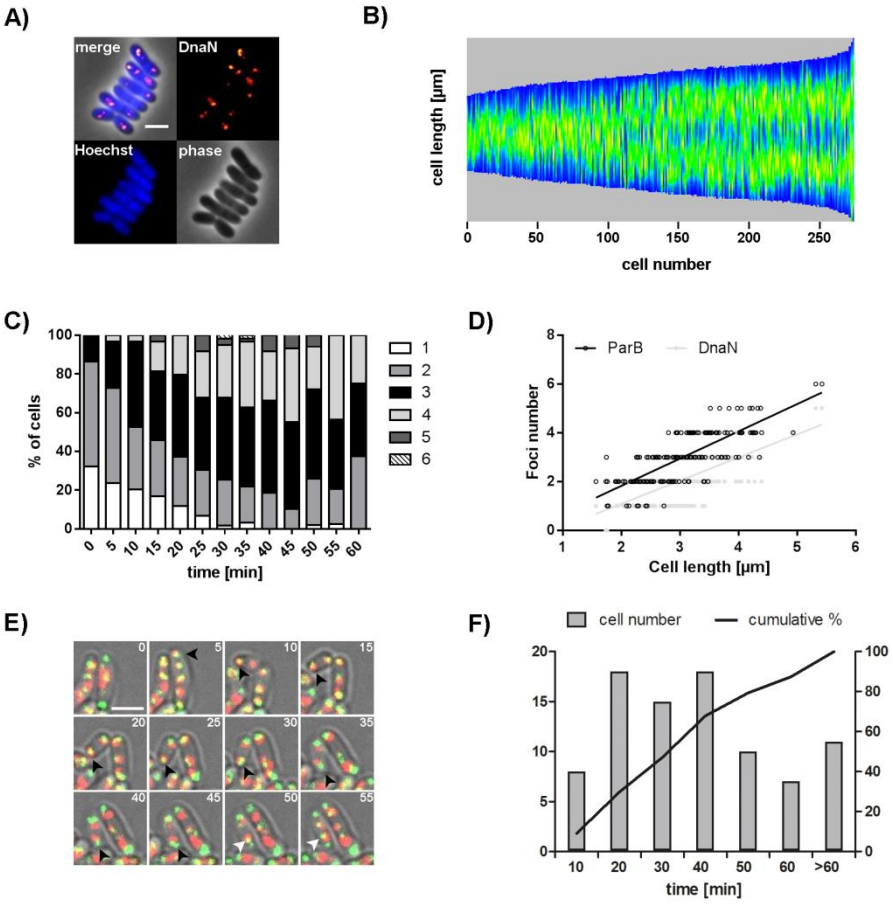

Figure 4. Dynamic localization of multiple replisomes in *C. glutamicum*.

A) Localization of replisomes in *dnaN::dnaN-mCherry* cells. Shown is the overlay (merge) of DnaN fluorescence (red) and DNA stained with Hoechst (blue) with the phase contrast image and separate channels (DnaN, Hoechst, phase). Scale bar, 2 µm. **B)** Timing of replication along the cell axis. Automated analysis of still images with DnaN-mCherry fluorescence. Cells are sorted by cell length and DnaN-mCherry fluorescence is shown as heat map (blue to orange) (n>250). **C)** Replisome number per cell varies within one cell cycle. Fraction of cells with 1-6 DnaN spots were determined for each time point (n=59). **D)** ParB and DnaN foci number in relation to cell length in *C. glutamicum parB::parB-eYFP dnaN::dnaN-mCherry* (n=200). Linear regression lines are shown, r(ParB-eYFP/DnaN-mCherry)=0.65. **E)** Time frames of

replication initiation until segregation of sister *oriC*s. Time series showing movement of ParB-eYFP and DnaN-mCherry foci (green and red, overlay in yellow) in *parB::parB-eYFP dnaN::dnaN-mCherry* cell. Images were taken in 5 min time-frames as indicated (top right corner). At time point 5 a replisome forms at polar *oriC* (black arrowheads); sister *oriCs* separate at time point 50 (white arrowheads). Scale bar, 2 µm. **F)** Variable cohesion periods of sister *oriC*s. Shown is the distribution of *oriC* colocalization times analyzed by time lapse microscopy together with the cumulative skew of sample data (n=88).

858 ——

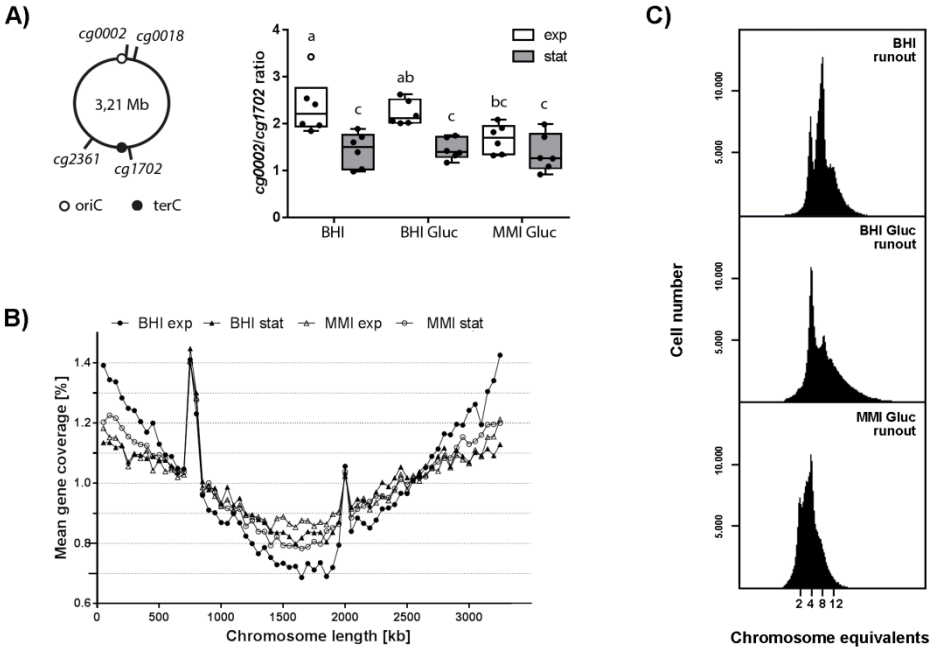

859

860 **Figure 5. Timing of DNA replication initiation and determination of *oriC***

861 **numbers per cell.**

862 **A)** Marker frequency analysis of *oriC* and terminus regions. Right: Schematic
863 representation of chromosomal positions of *oriC* and *terC* proximal marker genes
864 applied. Left: *oriC* to terminus ratios of the wild type strain grown under different
865 growth conditions were determined by frequency analysis of markers *cg0002* and
866 *cg1702* (see S4B for *cg0018*/*cg2361* ratios). Right: Cells were grown in BHI, BHI
867 supplemented with glucose or MMI supplemented with glucose. Samples were taken
868 in the exponential (white boxes) and stationary growth phases (gray boxes). Results
869 are shown as boxplots with medians indicated as solid lines and whiskers of 1.5 ×
870 interquartile range (n=6). An ANOVA yielded significant variation among conditions
871 growth phase ($F(1, 30)=28.00$, $p<.0001$) and medium ($F(2, 30)=3.43$, $p<.05$). Letters
872 indicate significant differences between data sets determined by Post-hoc Bonferroni
873 analysis at $p<.05$. **B)** Whole genome sequencing. Genomic DNA of *C. glutamicum*

874 wild type grown in BHI or MMI supplemented with glucose was isolated in
875 exponential and stationary growth phases. Data were analyzed by Illumina MiSeq®
876 shotgun sequencing and mapped to the *C. glutamicum* ATCC 13032 genome
877 sequence (GeneBankID: BX927147.1). Data are displayed as the mean gene
878 coverage in % of each 50-kb sliding window of the total mean coverage per sample.
879 Note that the RES167 strain used in this study features besides a lack of the phage
880 island (cg1981-cg2034) an *ISCg14* mediated 5 × tandem amplification of the *tus*
881 locus (peaks at approx. 750 and 2000 kb positions); both loci were excluded from
882 data analysis. Stable replication progression is evidenced by frequency of genes
883 between *oriC* (located at 0 kb) and terminus regions (at approx. 1.6 Mb). **C)**
884 Chromosome numbers per cell determined by flow cytometry after replication runout
885 in BHI, BHI supplemented with glucose or MMI supplemented with glucose.
886 Depending on growth conditions between 2 and 12 chromosomes were detected.

887

888

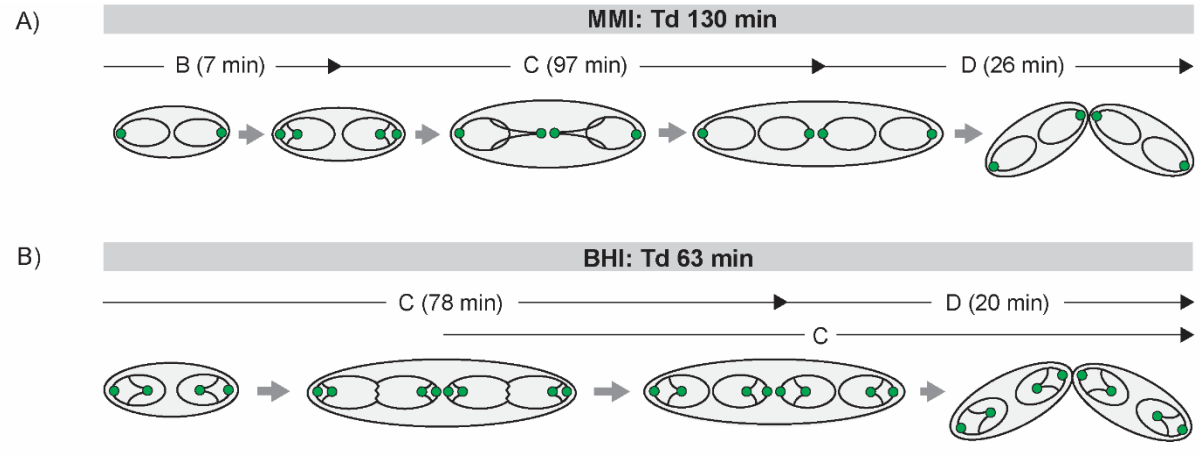

889

890 **Figure 6. Spatiotemporal chromosome organization of *C. glutamicum*.**

891 Chromosomes are depicted as black lines with *oriCs* as green circles. In newborn
892 cells two initial *oriC* locate close to the poles. Upon initiation of a new round of
893 replication sister origins segregate non-synchronously from polar ParB-eYFP cluster
894 and move towards midcell where a new septum is formed. Notably, stages with
895 single chromosomes per cell are absent. **A)** Cell cycle of slow growing cells in MMI
896 medium. A short B period is followed by C- and D-periods; replication takes place
897 within one generation. **B)** Chromosome organization during fast growth in BHI
898 medium. Multifork replication allows for short doubling times with a second round of
899 replication starting after the first half of the cell cycle, around 15 min before the
900 previous one terminates.

901

902 **Table 1. Overview of *C. glutamicum* cell cycle parameters at distinct growth**
903 **rates.**

Growth medium	μ [1/h]	T_d [min]	*oriC*/*terC*	*oriC*/cell	C [min]	D [min]
BHI	0.66	63	2.36 ± 0,54	5.90 ± 0,03	78	20
BHI Gluc	0.50	83	2.23 ± 0,21	5.17 ± 0,02	96	18
MMI Gluc	0.32	130	1.68 ± 0,28	3.85 ± 0,16	97	26

904

905

906 **Table 2. Speed of DNA replication forks summarized for different model**
907 **organisms.**

Organism	Genome size [Mb]	C-period [min]	Replication speed [bases/sec]	Reference
Corynebacterium glutamicum	3.21	78	340	this work
Mycobacterium tuberculosis	4.42	660	50	(85)
Mycobacterium smegmatis	6.99	140	400	(72,73)
Myxococcus xanthus	9.14	200	380	(70,86)
Caulobacter crescentus	4.02	95	350	(87)

Vibrio cholerae*	2.96	30-50	490-820	(17,88)
Bacillus subtilis	4.22	50-60	600-700	(67,89)
Escherichia coli	4.64	40-200	200-1000	(15,67,90-92)

908 *Shown are parameters for chromosome I only.

909